Supporting information Figures

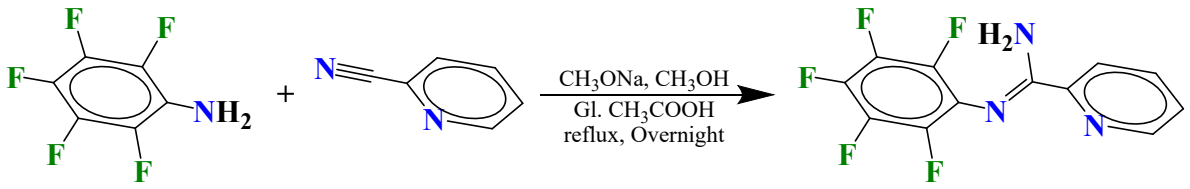

Scheme S1. Synthesis of ligand ((F5-Bn)Py), (L).

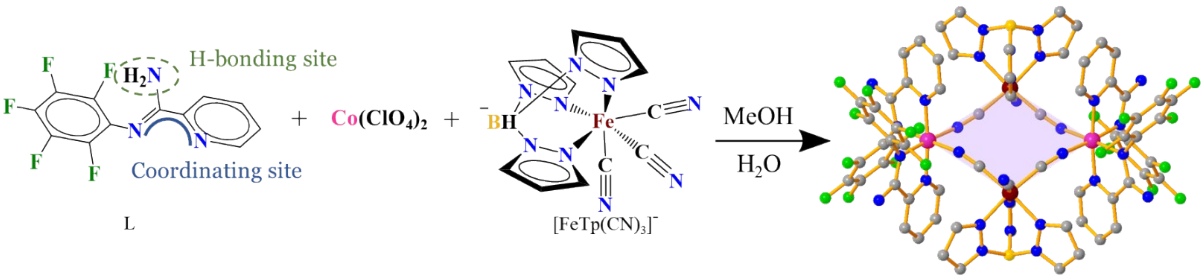

Scheme S2. Synthesis of $[Fe(Tp)(CN)_3]_2[Co\{L\}]_2(ClO_4)_2 \cdot 4MeOH \cdot 2H_2O$ (**1**$\cdot 4MeOH \cdot 2H_2O$).

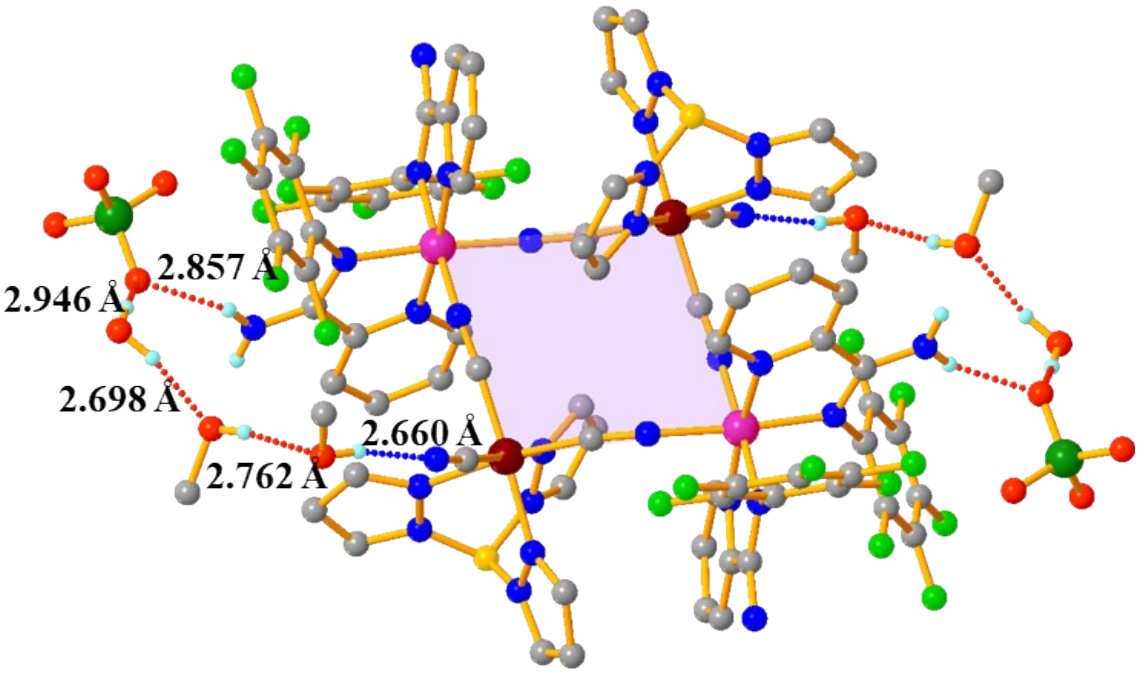

Figure S1. Crystal Structure of **1**$\cdot 4MeOH \cdot 2H_2O$. Colour Code: Green: Fe; Pink: Co; Blue: N; Grey: C; Yellow: B, Dark green: Cl, Light green: F. H-bonding interactions between the square complex, solvents and anions are shown with red dotted lines. The hydrogen not involved in H-bonding is omitted for clarity.

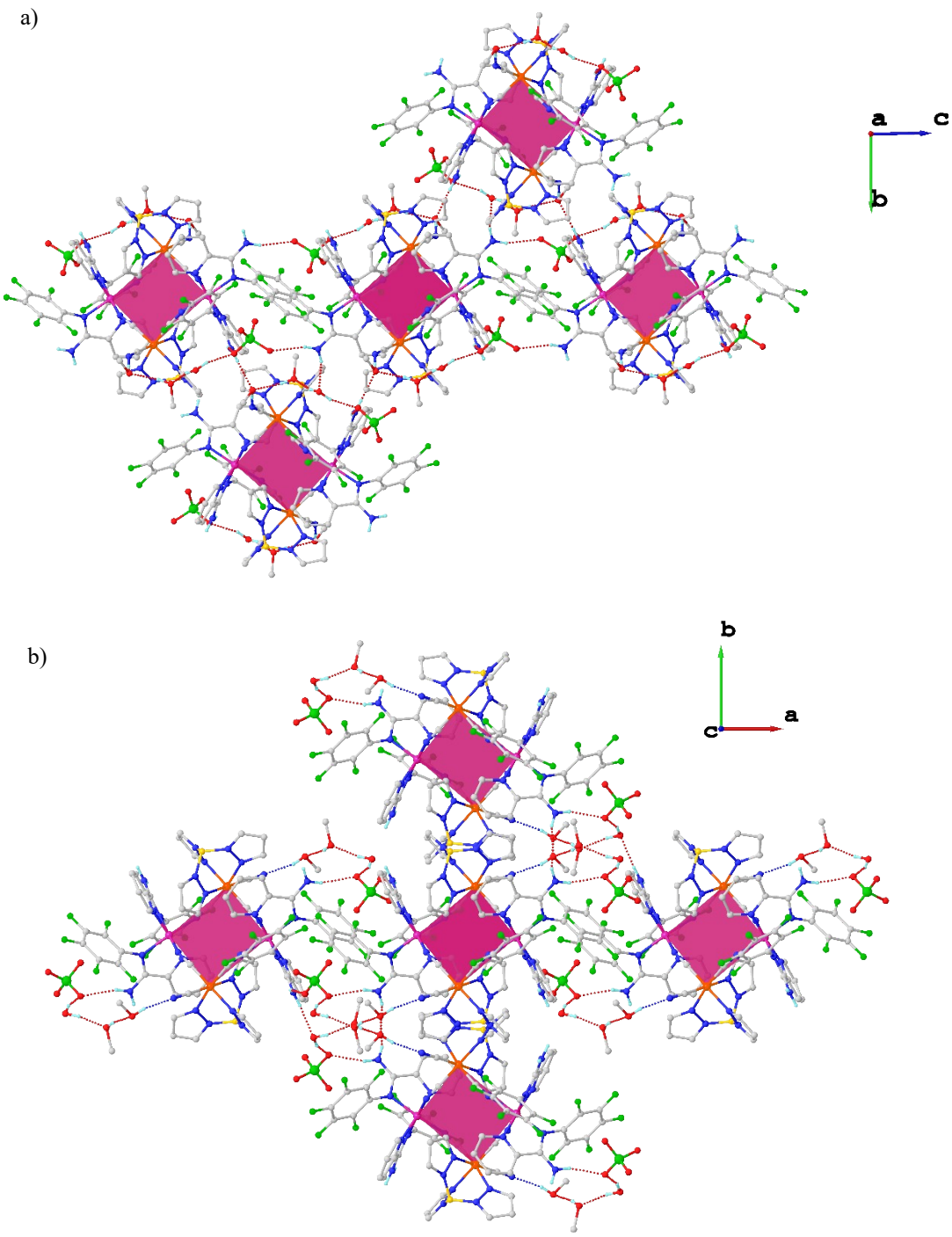

Figure S2. Hydrogen bonding interactions between solvent molecules, perchlorate anions and the $[Fe_2(\mu\text{-}CN)Co_2]$ square grids a) along *the bc* plane and b) along the *ab* plane in complex **1**·4MeOH·$2H_2O$. The Hydrogen atoms not involved in Hydrogen bonding have been omitted for clarity.

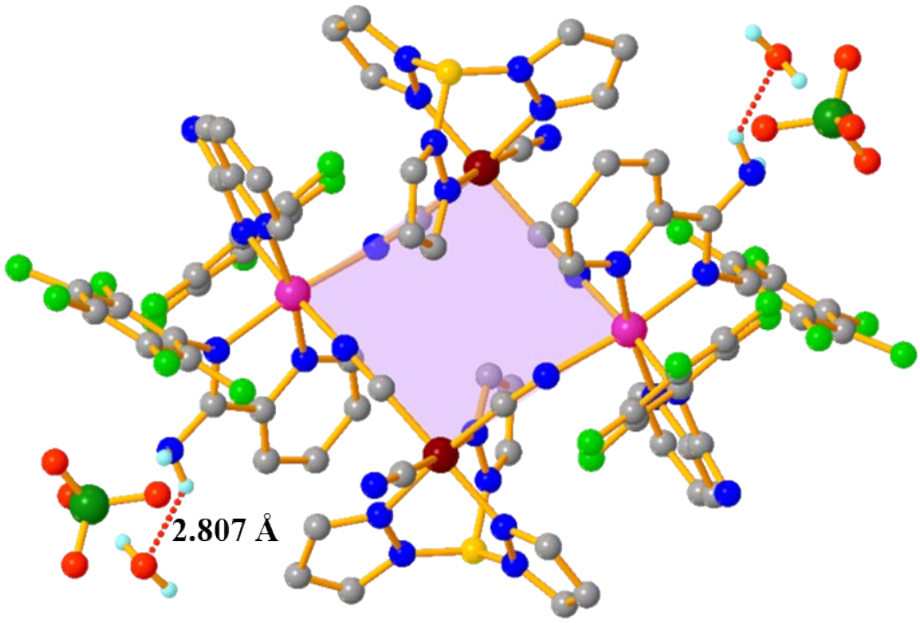

Figure S3. Crystal Structure of **1**·2H_2O. Colour Code: Green: Fe; Pink: Co; Blue: N; Grey: C; Yellow: B, Dark green: Cl, Light green: F. H-bonding interactions between the square complex, solvents and anions are shown with red dotted lines. The hydrogen not involved in H-bonding is omitted for clarity.

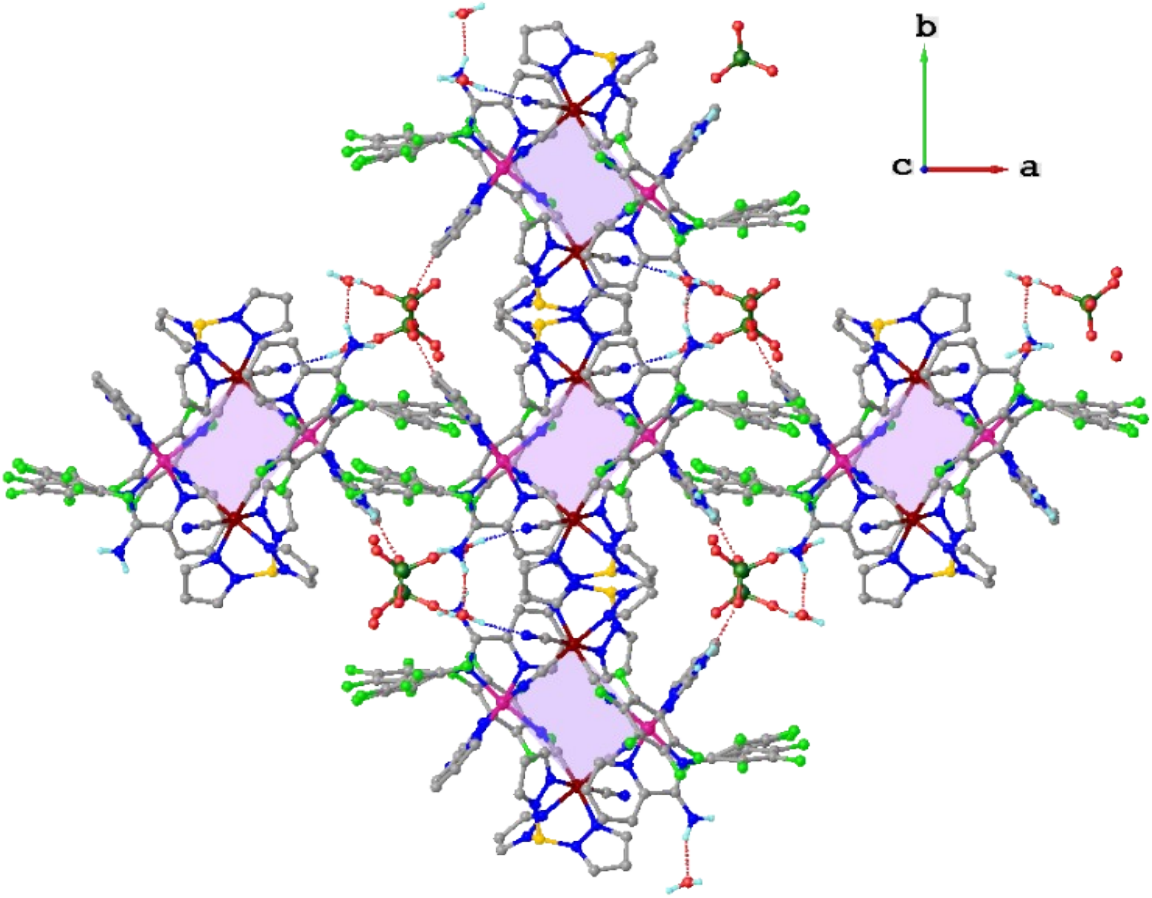

Figure S4. Hydrogen bonding interactions between solvent molecules, perchlorate anions and the [Fe_2(μ-CN)Co_2] square grids along the *ab* plane in complex **1**·2H_2O. The Hydrogen atoms not involved in Hydrogen bonding have been omitted for clarity.

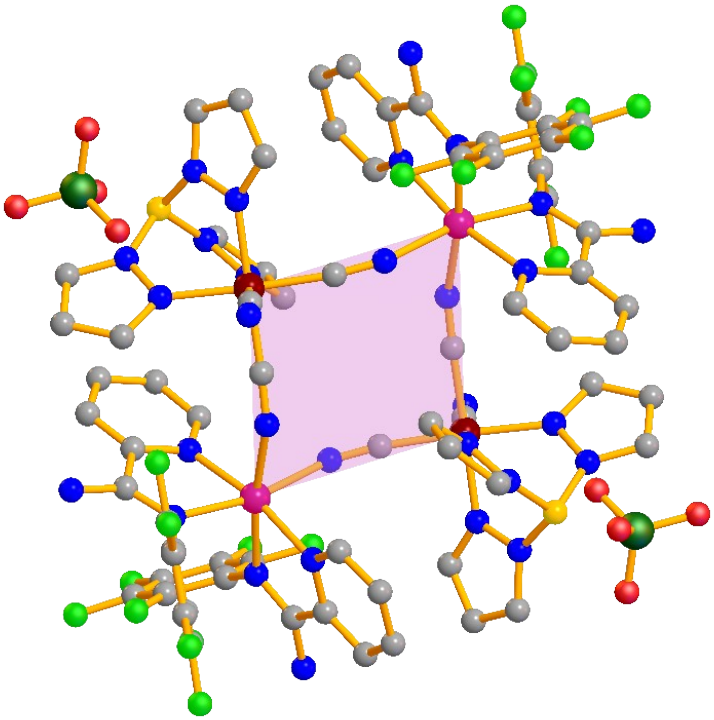

Figure S5. Crystal Structure of **1**. Colour Code: Green: Fe; Pink: Co; Blue: N; Grey: C; Yellow: B, Dark green: Cl, Light green: F. The hydrogen not involved in H-bonding is omitted for clarity.

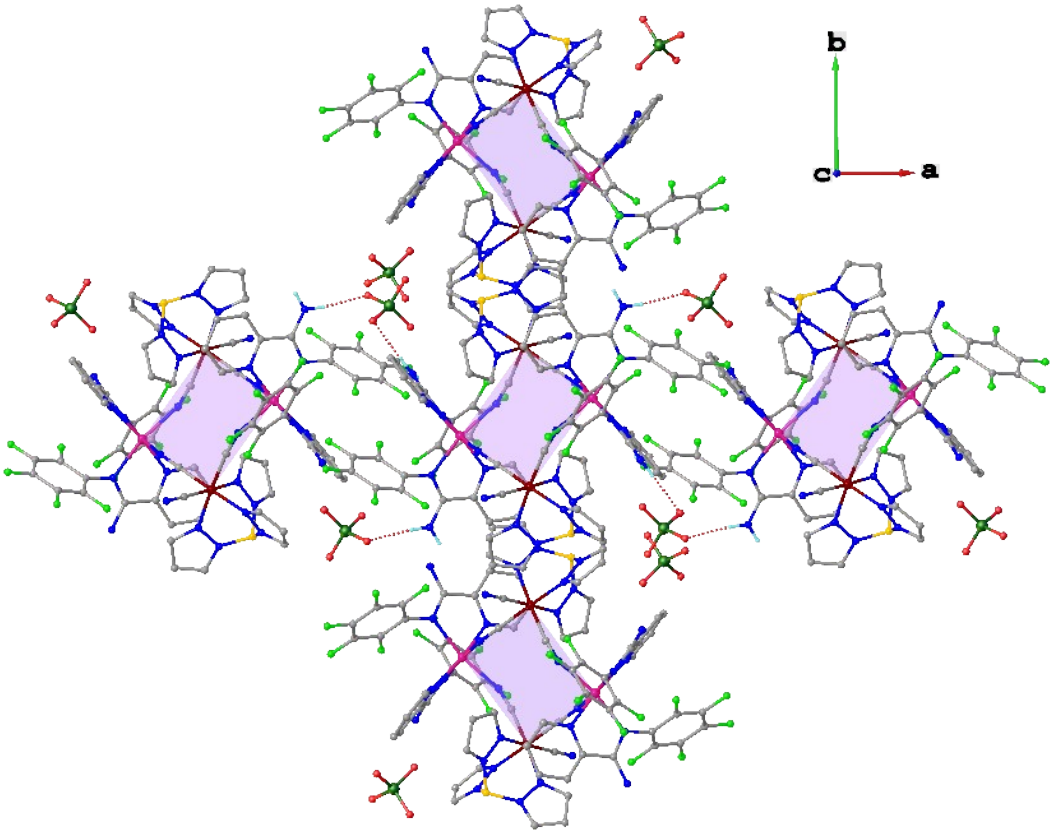

Figure S6. Hydrogen bonding interactions between solvent molecules, perchlorate anions and the $[Fe_2(\mu\text{-}CN)Co_2]$ square grids along the *ab* plane in complex **1**. The Hydrogen atoms not involved in Hydrogen bonding have been omitted for clarity.

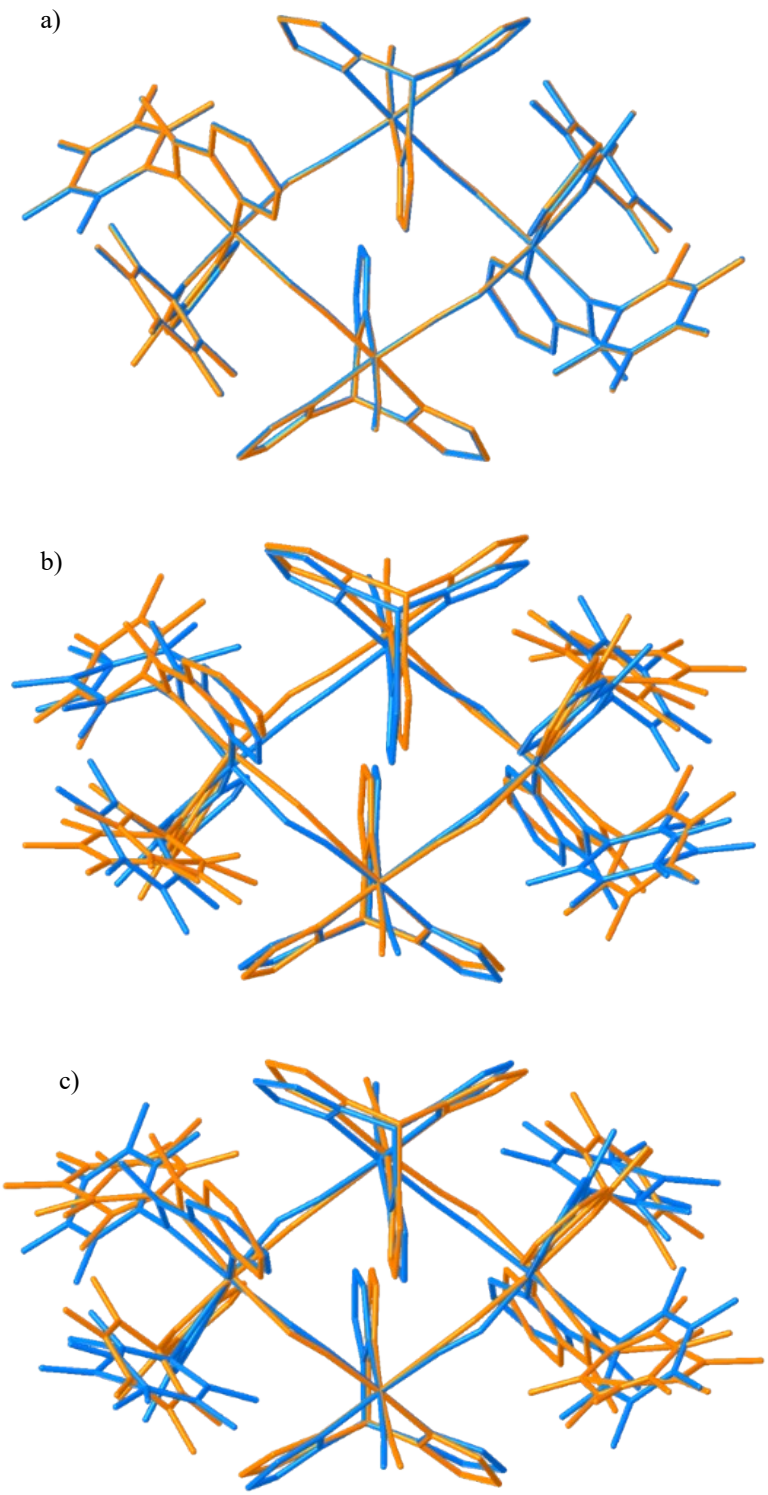

Figure S7. Overlay diagram of a) **1**·4MeOH·2H_2O (blue: 100 K, orange: 200 K) and b) **1**·2H_2O (blue: 140 K, orange: 200 K) and c) **1**·2H_2O (blue: 140 K, orange: 110 K). The Hydrogen atoms are omitted for clarity.

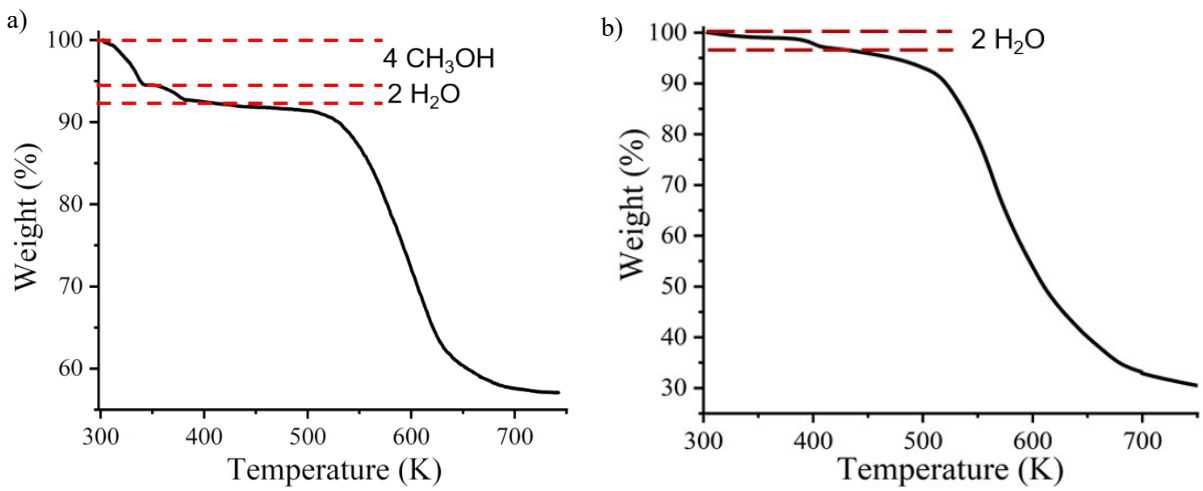

Figure S8. Thermogravimetric analysis of a) **1**·4MeOH·2H_2O, b) **1**·2H_2O and c) **1** representing loss of solvent molecules.

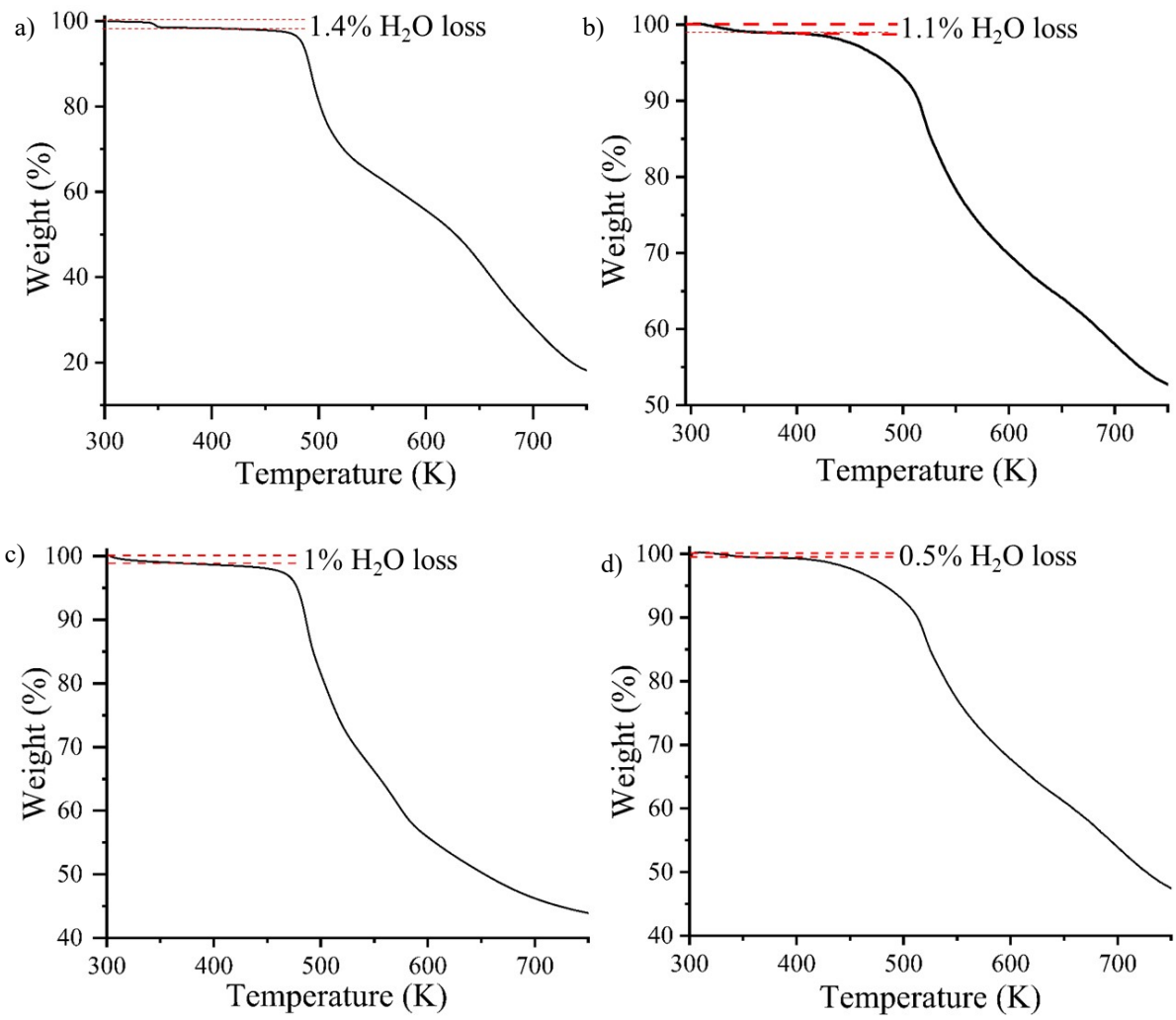

Figure S9. Thermogravimetric analysis of **1**·2H_2O after a) 2 days, b) 1 week, c) 2 weeks and d) 4 weeks.

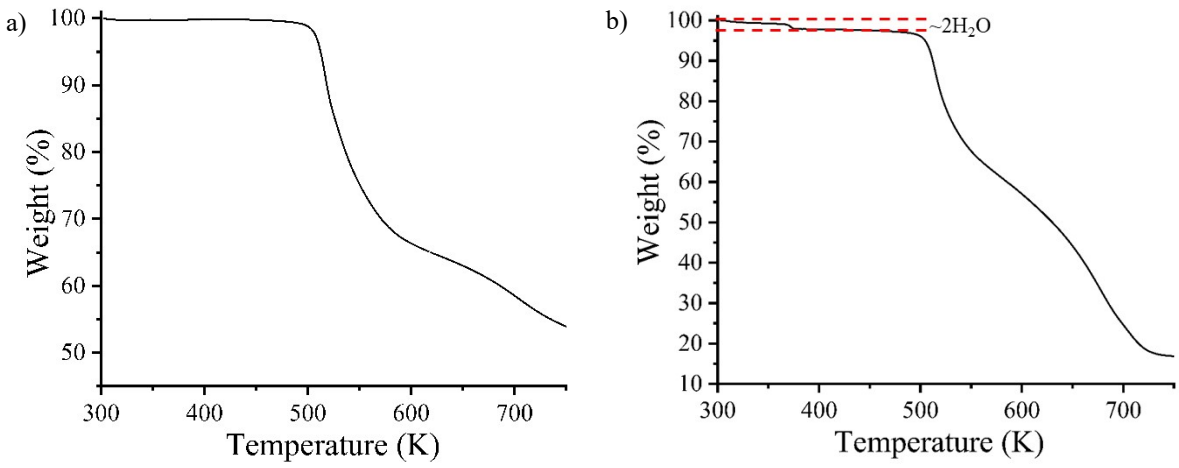

Figure S10. Thermogravimetric analysis of **1** (a) and resolvated complex (b).

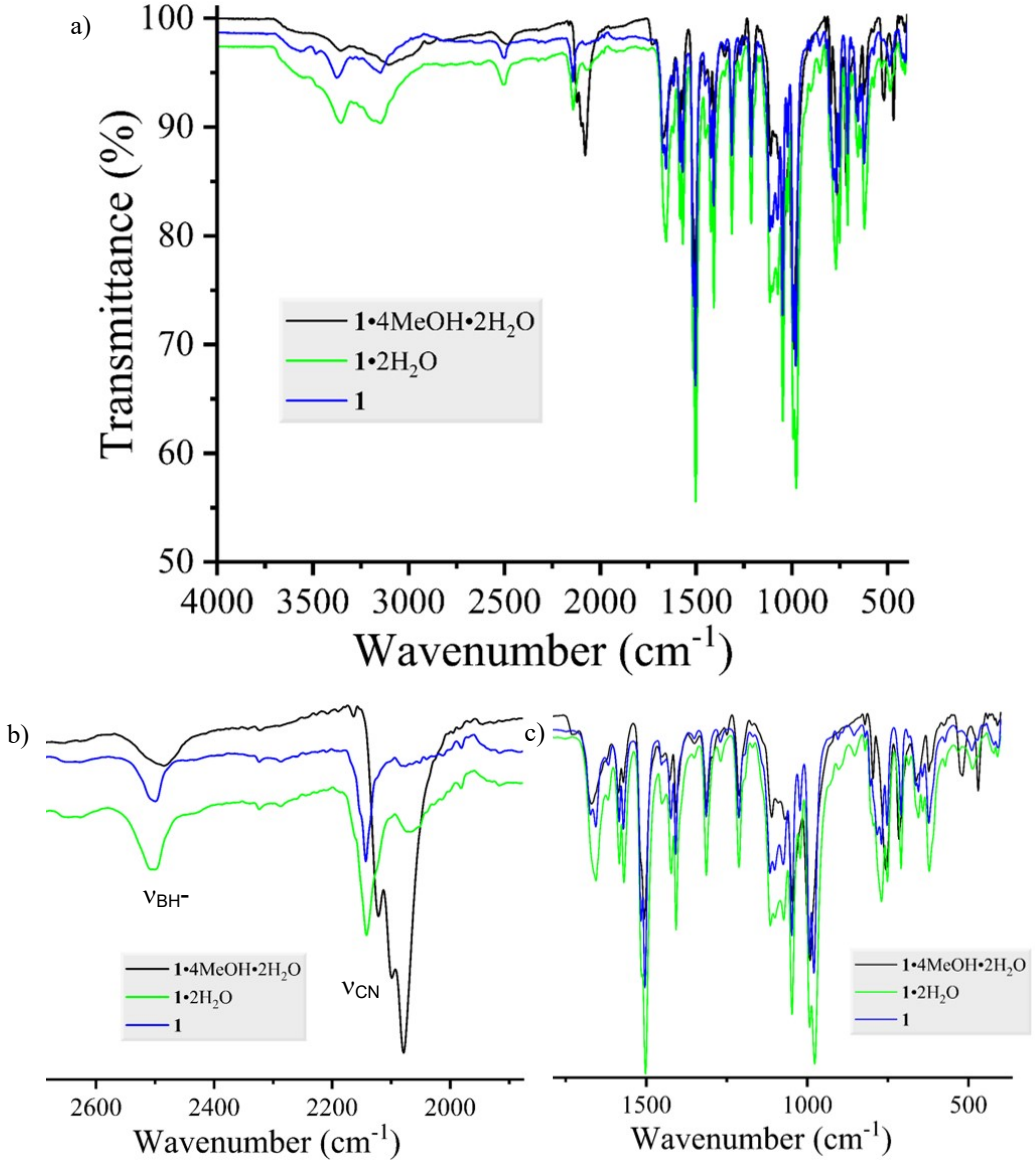

Figure S11. a) Infrared spectroscopy of **1**·4MeOH·2H_2O, **1**·2H_2O and **1**. Enlarged view of b) BH^- and CN frequency region and c) 1750 – 400 cm^{-1}**.**

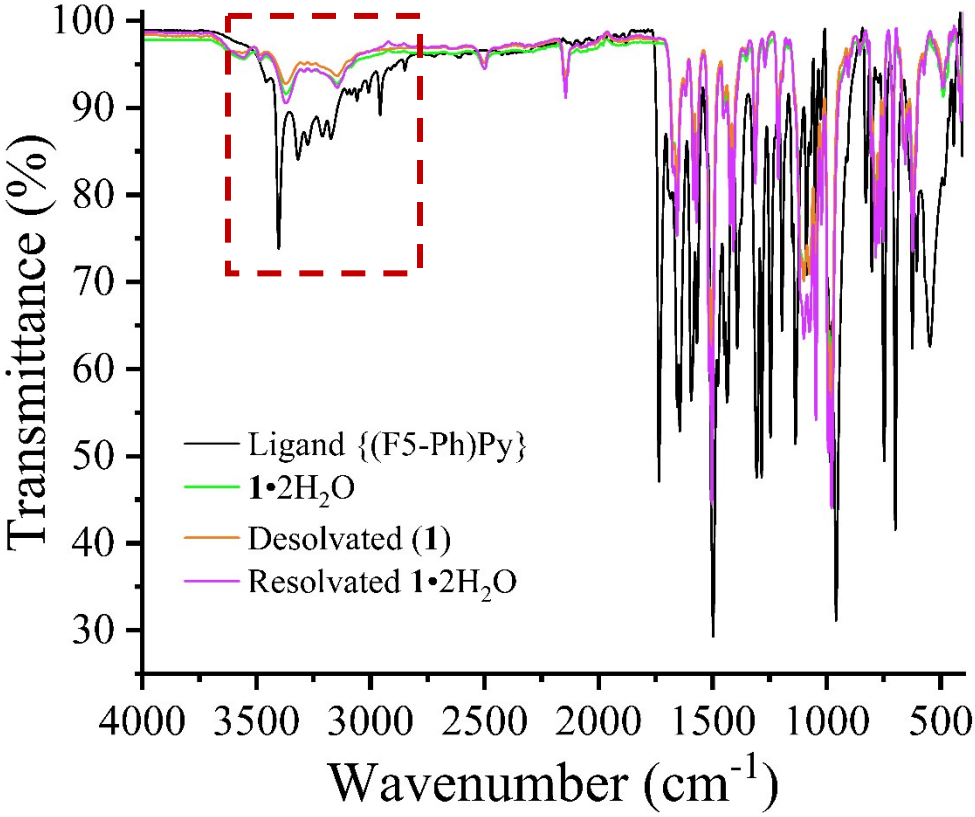

Figure S12. Infrared spectroscopy of ligand, **1**·$2H_2O$, desolvated and the resolvated complex.

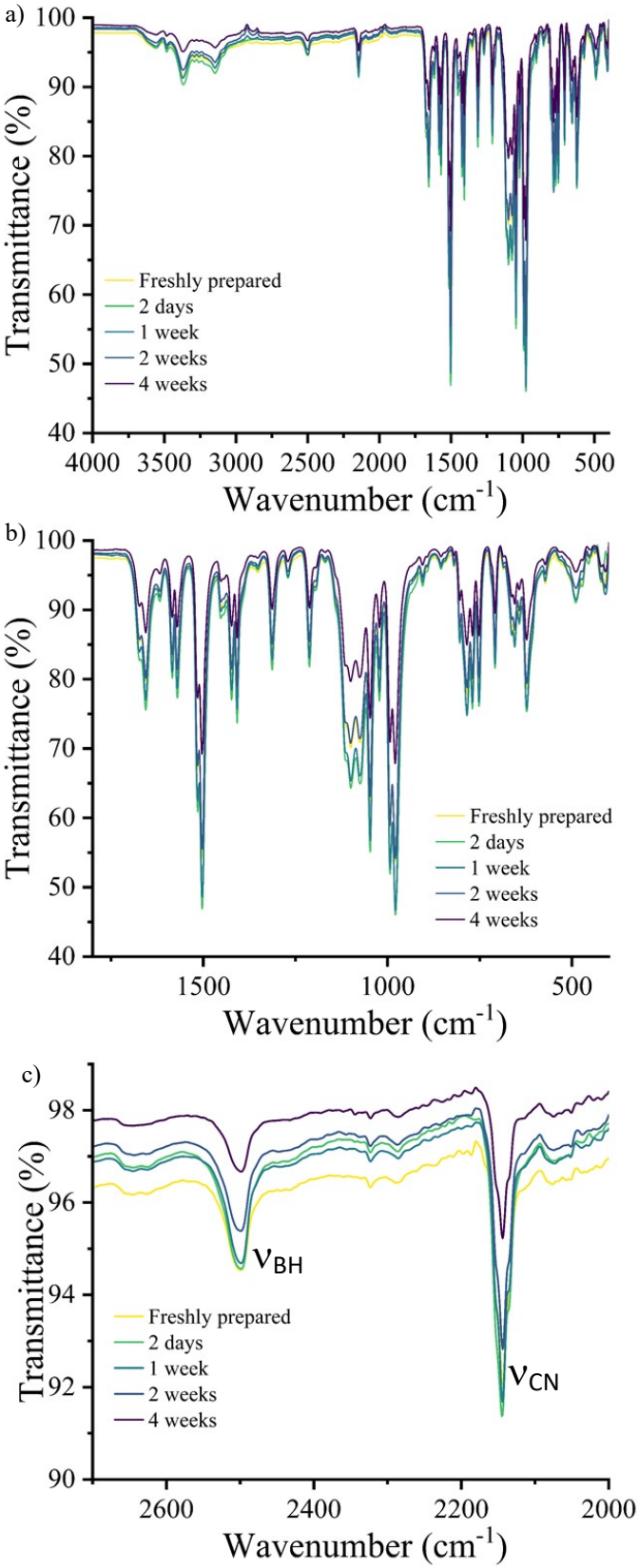

Figure S13. Infrared spectroscopy of **1**·$2H_2O$ with ageing a) complete spectra from 4000-400 cm^{-1}, b) fingerprint region (1800-400 cm-1), and c) ν_{BH} and ν_{CN} stretching frequencies.

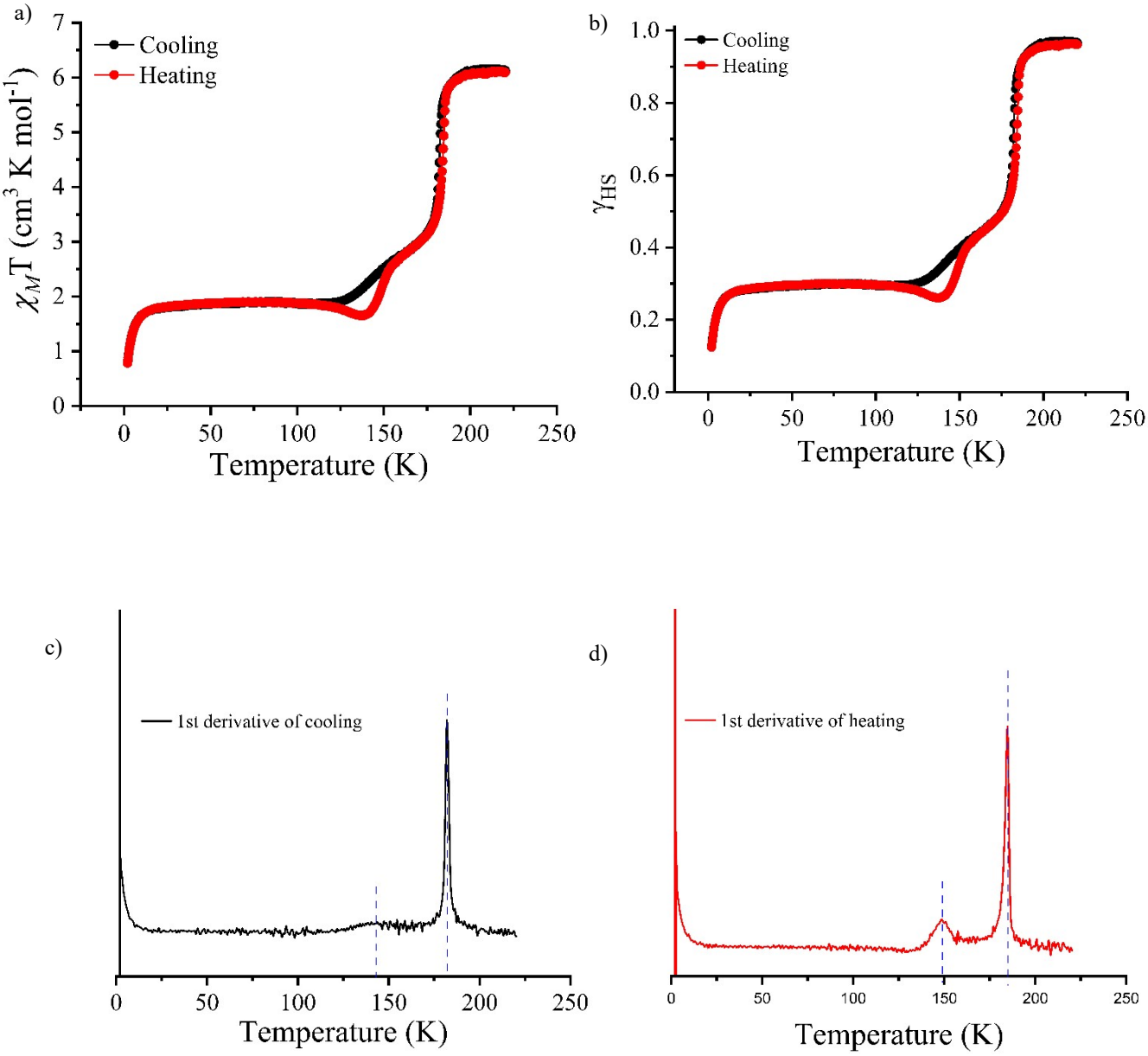

Figure S14. a) $\chi_M T$ *vs.* T (black), b)) γ_{HS} *vs.* T and c) and d) are the derivative plots during cooling and heating, respectively, for complex **1**·2H_2O at 5 K min^{-1} with applied DC field of 1000 Oe. The separate derivative plot for the complex during the cooling and heating cycle (b and c, respectively).

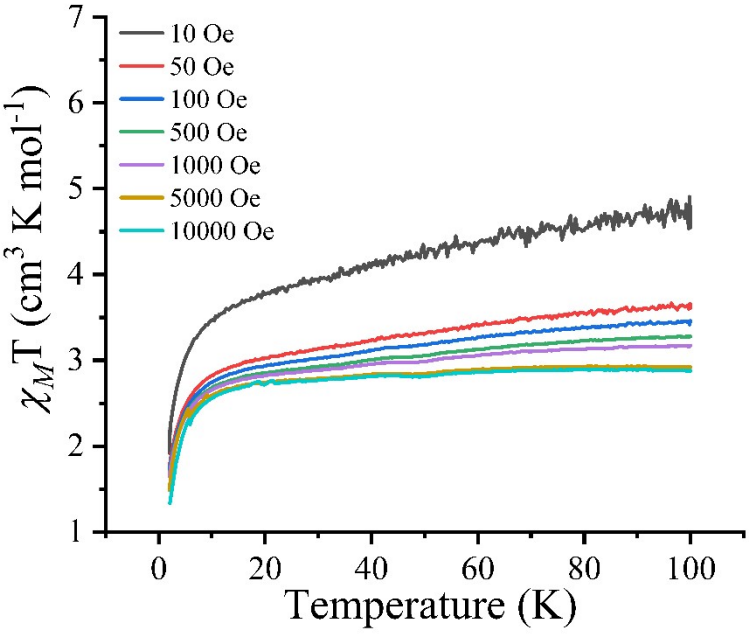

Figure S15. χ_MT *vs.* T plots for complex **1**·2H_2O at 5 K min^{-1} under different applied magnetic field from 10 Oe to 10000 Oe from 2-100 K.

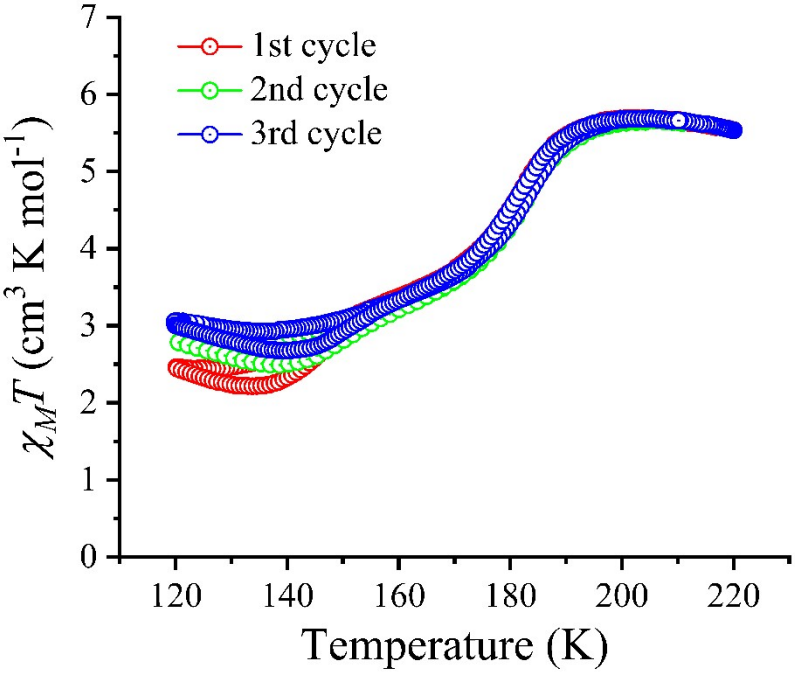

Figure S16. $\chi_M T$ *vs.* T plot at a scan rate of 5 K min^{-1} for complex **1**·2H_2O with three consecutive cycles upon resolvation.

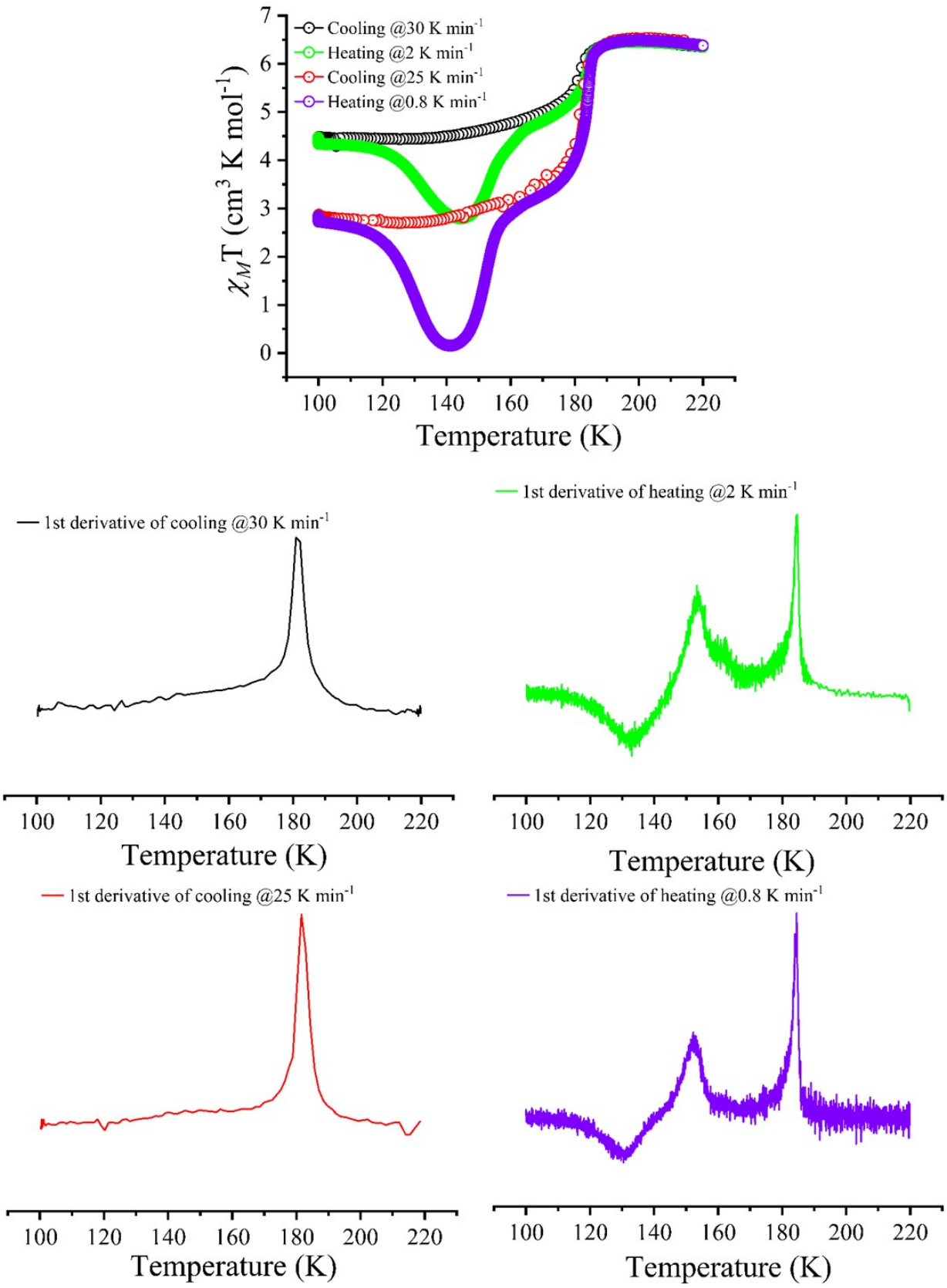

Figure S17. $\chi_M T$ *vs.* T plots for complex **1**·2H_2O upon thermal quenching with a scan rate of 25 K min^{-1} (black) and 30 K min^{-1} (red) via TIESST phenomenon. Heating was measured at a scan rate of 0.8 K min^{-1} (black) and 2 K min^{-1} (red). The 1st derivative plots during cooling and heating mode is shown in their representative colours with single-step and two-step transitions, respectively.

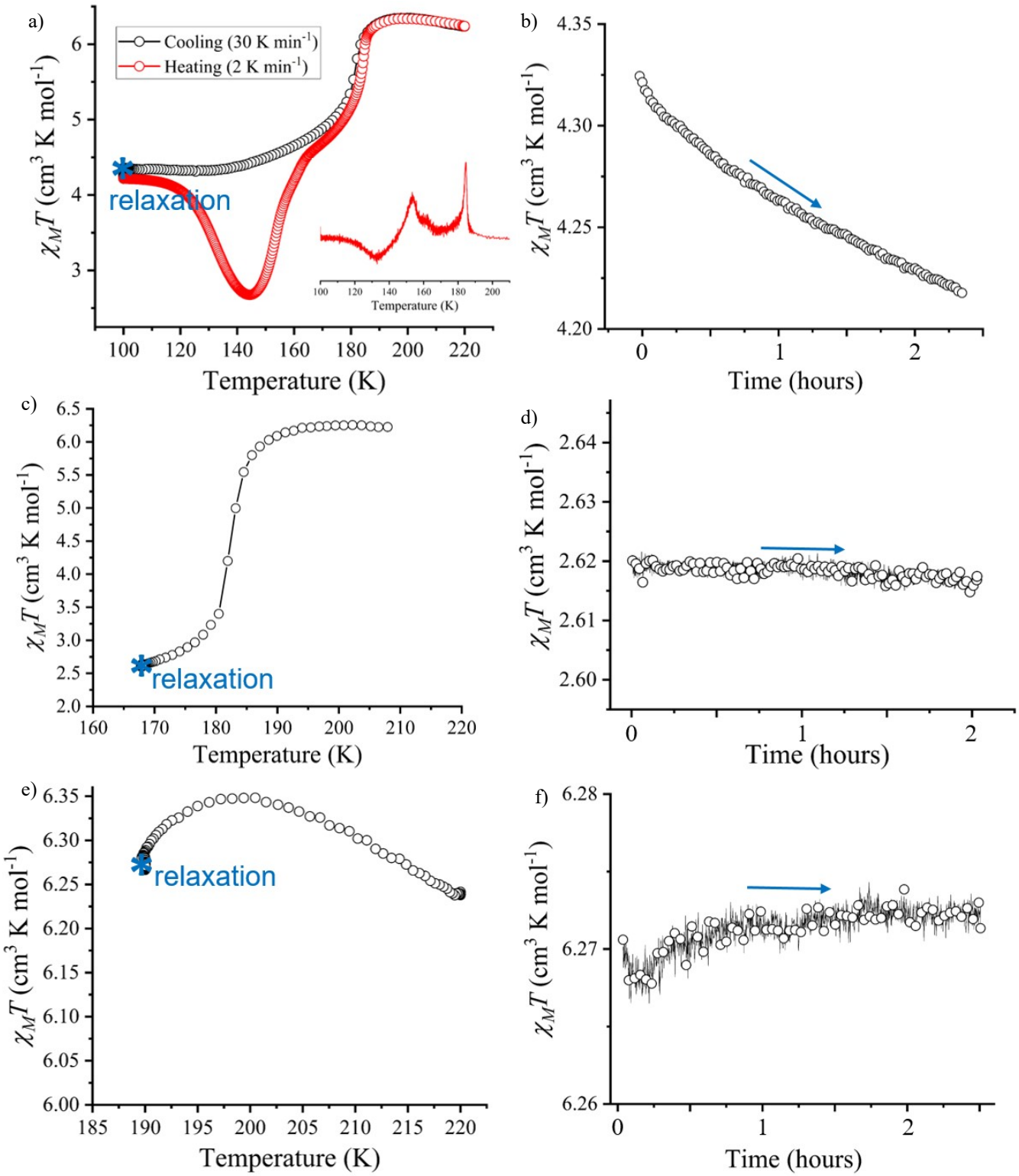

Figure S18. $\chi_M T$ *vs.* T plots for complex **1**•$2H_2O$ upon thermal quenching with a scan rate of 30 K min^{-1} upto a) 100 K, c) 168 K and e) 190 K followed by relaxation for about 2 hours at constant temperatures. b), d) and f) $\chi_M T$ *vs.* time plots at 100 K, 168 K and 190 K, respectively. Inset of a) shows the 1st derivative of heating cycle showing not so prominent three step-transition.

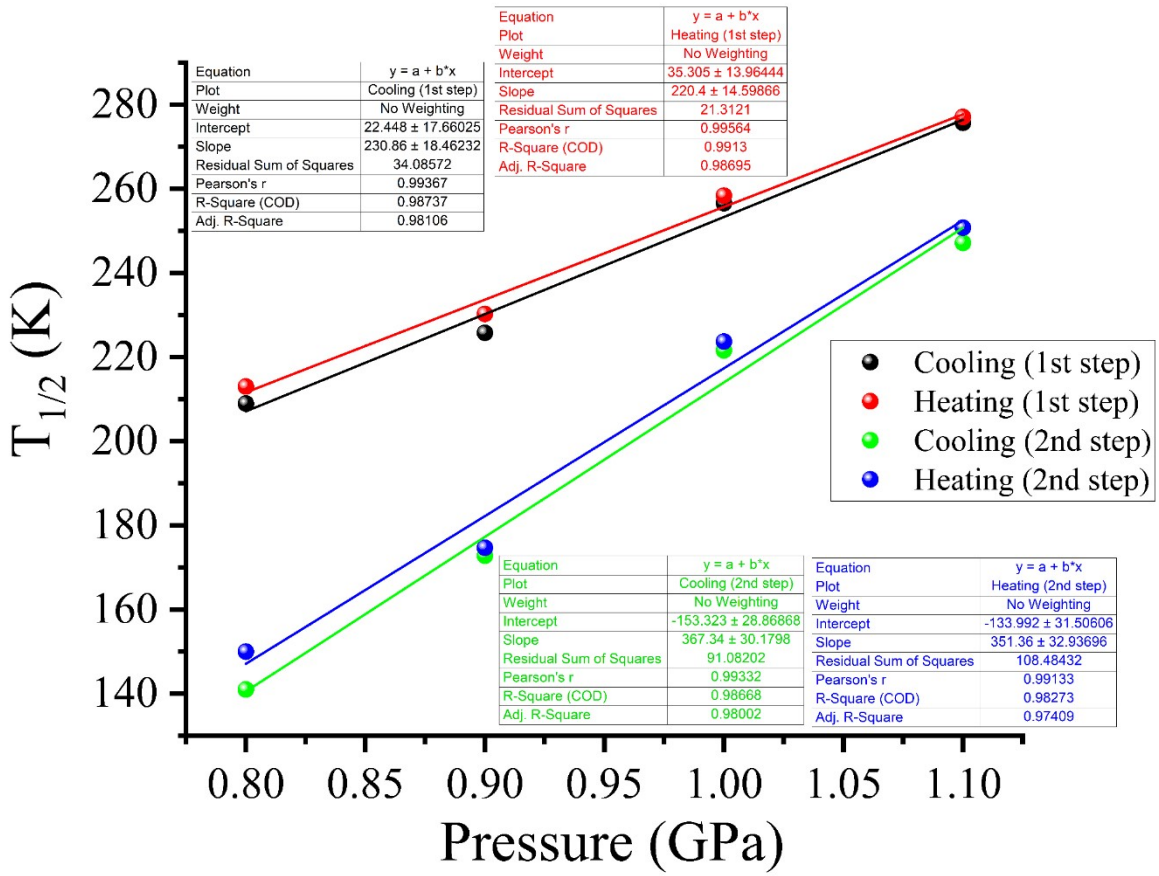

Figure S19. $T_{1/2}$ *vs.* Pressure plots for complex **1**·2H_2O showing linear relation above 0.8 GPa of threshold pressure, following Clayperon law.

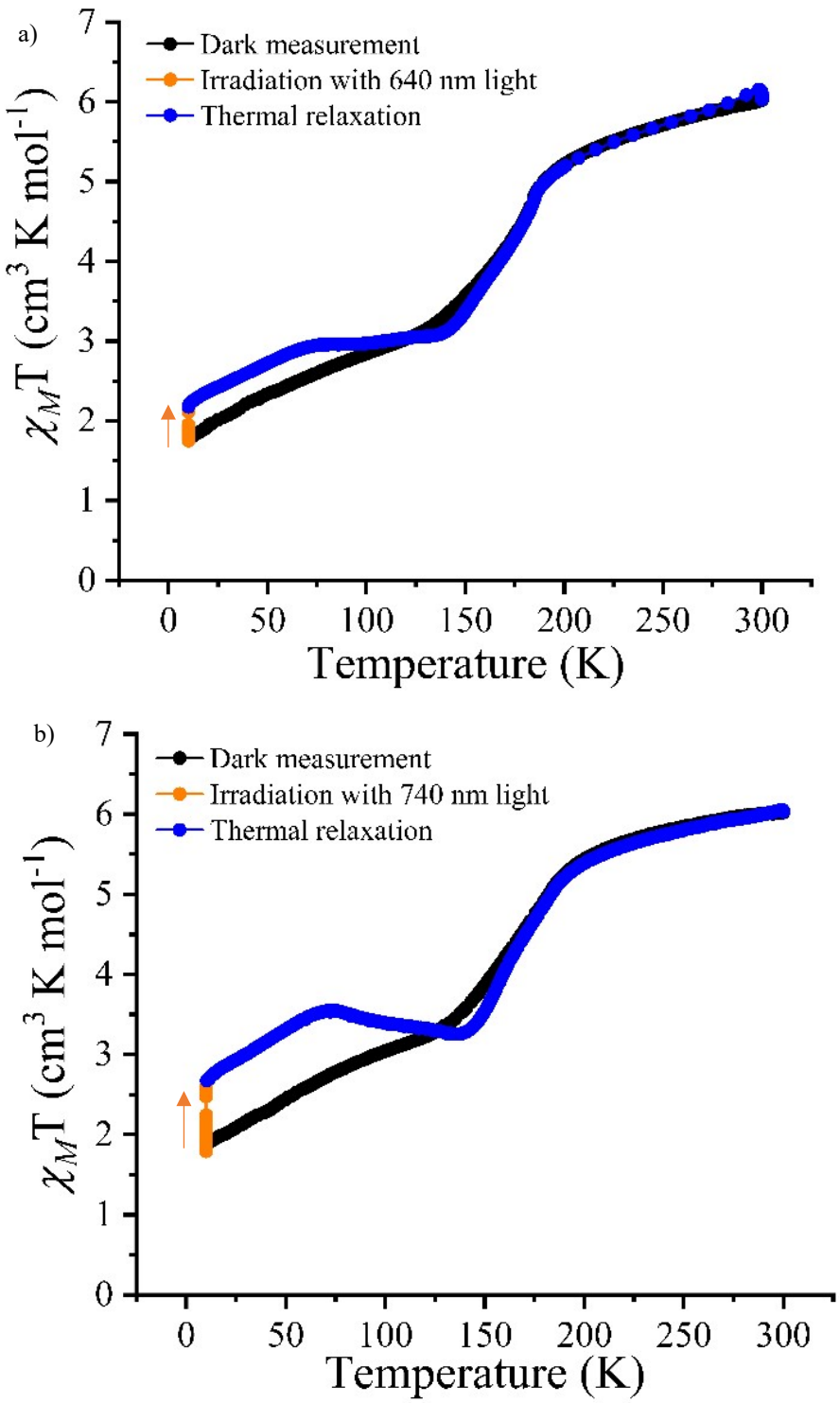

Figure S20. $\chi_M T$ *vs.* Temperature plots for complex **1**·2H_2O with irradiation with a) 640 nm and b) 740 nm of light (orange). The cooling rate is 5 K min^{-1} (black) and after irradiation, the heating is at 2 K min^{-1} (blue).